Biocompatibility of electrospun PVA-based nanocomposite with chemical vapor deposition-derived graphene monolayer

Hilal Turkoglu Sasmazel[1), *)] (ORCID ID: 0000-0002-0254-4541), **Marwa Alazzawi[2)]** (0000-0002-3617-6046), **Verra Sadhu[3)], Melike Gozutok[4)]**

DOI: https://doi.org/10.14314/polimery.2024.11.5

Abstract: The biocompatibility of electrospun PVA with monolayer graphene obtained by chemical vapor deposition (PVA/CVD-grown MLG) nanocomposite was investigated. The properties of PVA/CVD-grown MLG nanocomposite were compared with those of electrospun PVA mat. Raman analysis confirmed the presence of graphene monolayer on PVA. Although no significant changes in tensile properties were observed, the electrical conductivity increased from 0.1 (PVA mat) to 0.4 μS/cm (PVA/CVD-grown MLG). Thermal stability was also increased, as evidenced by the higher onset temperature and temperature of maximum decomposition rate determined by TGA. The contact angle decreased slightly, which resulted in higher PBS absorption and degradation of the nanocomposite. Water vapor transmission rate (WVTR) decreased from 40 (PVA mat) to 37 g/m^2 h (PVA/CVD-grown MLG). Cell culture studies showed better cell viability, population, and growth in the case of PVA/CVD-grown MLG nanocomposite due to improved physical, chemical and mechanical properties.

Keywords: electrospinning, monolayer graphene, CVD method, MG-63 cell, nanocomposites.

Biokompatybilność nanokompozytu na bazie elektroprzędzonego PVA z monowarstwowym grafenem otrzymanym metodą chemicznego osadzania z fazy gazowej

Streszczenie: Zbadano biokompatybilność nanokompozytu elektroprzędzonego PVA i monowarstwowego grafenu otrzymanego metodą chemicznego osadzania z fazy gazowej. Właściwości nanokompozytu porównano z właściwościami elektroprzedzonej maty PVA. Analiza Ramana potwierdziła obecność monowarstwy grafenu na PVA. Pomimo, że nie stwierdzono istotnych zmian właściwości mechanicznych przy rozciąganiu, to przewodnictwo elektryczne wzrosło z 0,1 (mata PVA) do 0,4 μS/cm (nanokompozyt). Zwiększyła się również stabilność termiczna, o czym świadczy wyższa temperatura początku rozkładu i maksymalnej szybkości rozkładu oznaczona metodą TGA. Nieznacznie zmniejszył się kąt zwilżania, co skutkowało większą absorpcją PBS i degradacją nanokompozytu. WVTR zmniejszył się z 40 (mata PVA) do 37 g/m^2·h (nanokompozyt). Ponadto ze względu na lepsze właściwości fizyczne, chemiczne i mechaniczne nanokompozytu uzyskano większą żywotność, populację i wzrost komórek.

Słowa kluczowe: elektroprzędzenie, monowarstwowy grafen, metoda CVD, ogniwo MG-63, nanokompozyty.

Electrospinning has been known as a technique to obtain nonwoven polymeric fibers using an electrical field to draw thin filaments. This technique is simple and does not require hot temperatures to maintain the polymer in the liquid state [1]. High surface areas, porosities, and micro-to-nanoscale fibers provide properties that other techniques cannot obtain. Therefore, electrospinning is utilized in tissue engineering, drug delivery, wound healing, and medical implant applications [2]. Recently, an electrospun scaffold-based tissue

[1)] Department of Metallurgical and Materials Engineering, Atilim University, Incek, Golbasi, Ankara, 06830, Turkey.

[2)] Freelance Researcher, Konyaalti, Antalya, Turkey.

[3)] Centre for Mechanical and Aerospace Science and Technologies (C-MAST), Universidade da Beira Interior, Rua Marques d'Avila e Bolama, 6201-001, Covilha, Portugal.

[4)] Head of R&D, Plasmagear Inc, Montreal, Quebec, H2V4L5, Canada.

[*)] Author for correspondence: hilal.sasmazel@atilim.edu.tr

engineering approach has emerged as a promising strategy [3].

Graphene is a two-dimensional material composed of a single layer of carbon atoms arranged in a hexagonal lattice. This unique structure gives rise to its remarkable properties, including exceptional electrical conductivity, high thermal conductivity, impressive mechanical strength, and a large surface area. While its biocompatibility is still under investigation and varies depending on factors like lateral size and surface functionalization, graphene holds promise for various biomedical applications, including drug delivery and tissue engineering [4]. However, the biocompatibility of graphene can be enhanced through various methods, such as chemical vapor deposition [5]. This process not only improves the biocompatibility of graphene but also offers affordability and mass production capabilities compared to conventional techniques [6–8]. As a result, graphene has found widespread use in diverse applications, including packaging, electrical and thermal applications, tissue engineering, filtration, automotive, aerospace, and defense industries [9–11]. The synthesis of CVD-grown MLG involves placing a metal substrate, such as copper, into a furnace and heating it under a low vacuum to around 1000°C. This heat treatment anneals the copper, increasing its domain size. Afterward, methane and hydrogen gases are introduced into the furnace. The hydrogen catalyzes a reaction between the methane and the metal substrate surface, leading to the deposition of carbon atoms from the methane onto the metal surface through chemical adsorption. Finally, the furnace is rapidly cooled to prevent the deposited carbon layer from aggregating into bulk graphite. The high-quality CVD-grown MLG obtained has the potential to be utilized in numerous applications, including filtration, electrical applications, sensors, electrodes, nanoengineering, and bioengineering [12, 13]. For instance, Osikoya *et al*. have developed a highly ordered graphene-enzyme electrode using CVD for electrochemical biosensing application [14]. Furthermore, Ji *et al*. [15] have created transparent conductive films by doping CVD-grown graphene with vanadium oxide.

Polyvinyl alcohol is a versatile, linear, semicrystalline polymer known for its distinctive properties. Its structure, characterized by a carbon backbone and pendant hydroxyl functional groups, contributes to its unique attributes. PVA readily dissolves in water, enabling the formulation of solutions that can be easily processed into various forms, including fibers and coatings. Beyond its solubility, PVA demonstrates a valuable affinity for fiber formation. This characteristic enables its use in diverse applications, such as the creation of textile fibers and biomedical scaffolds. While considered biodegradable, the rate of PVA degradation can vary, prompting ongoing research to enhance this characteristic. Notably, PVA is recognized as non-toxic and biocompatible, making it suitable for applications involving contact with food or human tissue [16]. Developing nanocomposites incorporating PVA and CVD-grown graphene has recently garnered significant interest from researchers and engineers. For instance, a study by Barzegar *et al*. [17] involved the fabrication of hollow nanocomposites through the electrospinning of PVA and CVD-grown graphene, and they reported that the resulting nanocomposites exhibited enhanced electrical, thermal, and mechanical properties.

In the present study, the nanocomposite was synthesized by electrospinning PVA on CVD-produced graphene monolayer. The graphene monolayer was initially produced on a copper film, which was then integrated into the electrospinning system as a collector. Then, the graphene was separated by peeling the electrospun PVA from the copper film, which resulted in the transfer of graphene. The graphene layer was successfully peeled off from the copper film using this technique. This approach is a non-etching, simple and cost-effective method compared to other graphene transfer techniques reported in the literature. Optical microscopy and scanning electron microscopy analysis were performed to confirm the attachment of the graphene layer. Furthermore, Raman spectroscopy was used to confirm the presence of graphene. In addition, the fiber morphology and mechanical properties of the nanocomposites were evaluated. The thermal properties and electrical conductivity of the nanocomposites were determined by thermogravimetric analysis and a 4-point probe measurement system, respectively. In addition, the surface wettability, PBS absorption, shrinkage, in vitro degradation, and water vapor transmission rate of the nanocomposites were evaluated. For the first time in the literature, the in vivo cellular interactions of the obtained nanocomposites were investigated by a cell culture study, which included MTT assay, alkaline phosphatase activity evaluation, Alizarin Red staining, and fluorescence microscopy analyses.

EXPERIMENTAL PART

Materials

Nanotechnology Research and Application Center (SUNUM) at Sabanci University obtained CVD-grown MLG. PVA (molecular weight 85 000–124 000 g/mol and HD, 87–89%) was used without further purification and purchased from Sigma-Aldrich (Burlington, MA, USA). Phosphate buffer (PBS) was obtained from Amresco (USA). Materials used in cell culture studies were purchased from Amresco (USA), including BSA (bovine serum albumin), Dulbecco's modified Eagle's medium (DMEM/F12), penicillin/streptomycin, fetal bovine serum (FBS), ethanol (96%, v/v). Alizarin red-S and alkaline phosphate kits and 4′,6-diamidino-2-phenylindole dihydrochloride (DAPI) dyes were purchased from Sigma-Aldrich (USA).

Nanocomposites preparation

PVA mat and MLG were prepared by the method described in the literature [18]. 2 g of PVA powder and

30 mL of distilled water were stirred with a magnetic stirrer at 90°C for 3 h. The obtained solution was then electrospun under the following parameters: 20 cm distance between the needle and the collector, applied voltage of 20 kV and feed rate of 6.7 μl/min. In the meantime, a graphene monolayer was first synthesized using CVD technique to prepare MLG nanocompounds. Briefly, a 25 μm thick copper film was used as a catalyst as described in the literature [19]. The copper was cut into pieces, placed in a quartz chamber, heated to 1035°C under vacuum with 80 standard cubic centimeters of hydrogen per minute and annealed for 30 min. Then, a methane gas flow of 40 cm^3/min was introduced along with the hydrogen flow. After 30 min, the hydrogen flow was used to cool the chamber to below 100°C. Finally, the CVD-MLG-coated Cu film was mounted on the collector of the electrospinning machine, and the prepared PVA solution was electrospun onto the CVD-MLG using the same process parameters. The electrospinning process was carried out at room temperature.

Crosslinking of the fabricated nanocomposites

Polyvinyl alcohol is recognized as a highly water-soluble synthetic polymer [20]. Consequently, to create a stable and robust electrospun nanofibrous structure, the fabricated nanocomposites were subjected to crosslinking. A UV-340 lamp with a wavelength of 253.7 nm and an output power of 30 W was utilized to crosslink the fabricated nanofibers, employing different durations. To optimize the appropriate crosslinking duration, the fabricated samples were immersed in water and PBS solutions for the durations.

Methods

Thickness

A digital micrometer with a precision of 0.001 mm was utilized to measure the thickness of the fabricated PVA mat and PVA/CVD-grown MLG nanocomposite. The average of six measurements from each sample across different sample batches was calculated. The thickness of the obtained samples was in the range of 0.052–0.054 mm for both the electrospun PVA mat and the PVA/CVD-produced MLG nanocomposite.

Morphology

To investigate the formation of a graphene monolayer on a Cu film, light microscopy images of CVD-grown MLG on a Cu film were obtained using an Omano microscope (Virginia Beach, VA, USA). Furthermore, optical microscopy images of CVD-grown MLG were compared with those of the film.

The surface morphology of the fabricated PVA mat and PVA/CVD-grown MLG nanocomposite was examined using a Quanta 400F scanning electron microscope (Thermo Fisher Scientific, Eindhoven, The Netherlands). Square samples of 0.5 cm side were coated with a thin layer of gold before being placed in the SEM vacuum chamber. The average fiber diameter and pore size of the samples were determined using ImageJ Launcher. At least 30 measurements were taken from eight different images of each sample, and the data were statistically analyzed using JStats 1.8. A p-value of less than 0.05 was considered statistically significant by all analyses.

Tensile properties

Tensile properties were determined according to ISO 527-3 using a Zwick/Roell 250 kN universal tensile tester (Ulm, Germany) equipped with a 100 N load cell at crosshead speed of 10 mm/min under ambient conditions. Before tensile testing, the samples were cut into dog bone shapes. The mechanical properties of the PVA/CVD-grown MLG nanocomposites were then compared with those of electrospun PVA mats.

Thermal properties

Thermal properties of the samples were evaluated using a thermogravimetric analysis instrument (Perkin Elmer Pyris 1 TGA, USA). The TGA profiles were investigated under a nitrogen gas atmosphere with a heating rate of 10°C per minute, spanning a temperature range from 25°C to 700°C. The TGA results of the PVA/CVD-grown MLG nanocomposites were compared to those of the electrospun PVA mats.

Raman spectroscopy

A confocal Raman spectrometer (Renishaw inVia, Wotton-under-Edge, UK) was used to examine the Raman spectra of PVA mat, pure CVD-grown MLG and PVA/CVD-grown MLG. The Raman spectra peaks were examined using an incident laser beam at 532 nm.

Electrical conductivity

Electrical conductivity was assessed using a 4-point probe device (Keithley 220, USA). Conductivity was measured at least three separate locations on the sample. Additionally, the conductivity of an electrospun PVA mat was assessed as a control.

Contact angle

The water contact angle of the electrospun PVA mat and the PVA/CVD-fabricated MLG nanocomposite was measured by evaluating the angle of water droplet on the surface of the fabricated samples. A Phoenix 300 contact angle measurement system (South Korea) was used. Each sample was tested at room temperature at three separate

locations, and then the results were averaged using JStats 1.8 software. The wettability of the fabricated materials was compared with that of commercial tissue culture polystyrene.

PBS absorption and shrinkage tests

The samples were cut into 10 × 5 mm rectangles to evaluate their shrinkage and PBS absorption characteristics. The samples were then immersed in 20 mL of PBS (pH = 7.4) and incubated at 37.0°C for 24 h. After incubation, the samples were removed, and the excess surface water was drained using filter paper. The weight of the samples was measured, and Equation 1 was used to calculate the PBS absorption, where A is the PBS absorption (%) and W_0 (g) and W_1 (g) are the weight of the sample before and after PBS immersion.

$$A(\%) = \frac{W_1 - W_0}{W_0} \cdot 100 \quad (1)$$

To determine the shrinkage percentage, the samples were dried in a vacuum oven for 12 h after PBS incubation to remove excess water. The surface area was then measured before and after the incubation period, and the change ratio of the surface area was calculated to evaluate the shrinkage. Three samples from each group were recovered and analyzed after the PBS incubation.

***In vitro* degradation**

In vitro degradation analyses were conducted according to ASTM F1635-04 standard. The samples were weighed and then immersed in test tubes containing 0.1 M phosphate-buffered saline at pH 7.3, with the addition of 58.1 units/mL of lysozyme, and incubated at 37°C. After 1, 30, 60, 90, 120, 150, and 180 days of incubation, the samples were removed from the medium, washed with distilled water, and dried in a vacuum oven for 24 h to remove any excess water. The samples were then weighed, and the weight remaining was calculated using Equation 2.

$$Weight\ remaining(\%) = 100 - \left(\frac{W_0 - W_d}{W_0} \cdot 100\right) \quad (2)$$

W_0 represents the initial weight, and W_d denotes the final weight after the specific incubation intervals.

Water vapor transmission rate (WVTR)

The water vapor transmission rate of the fabricated samples was measured according to ASTM E96/E96M standard [21]. The prepared samples, measuring 2 mm in thickness and 50 × 50 mm in dimensions, were used to seal a water flask with a 50 mm diameter, filled with 10 mL of distilled water. The sealed cups were then incubated at 37°C for 24 h. The WVTR results were calculated using Equation 3 after measuring the weight of the water before and after the incubation period:

$$WVTR = \frac{W_0 - W_f}{A \cdot 24} \cdot 10^6 \quad (3)$$

where: A is the area of the flask's mouth, and W_0 and W_f are the bottle weights before and after incubation, both in grams.

Cell cultivation

Cell culture experiments were performed using human osteosarcoma cell line MG-63 (ECACC 86051601) to investigate cell interactions with PVA/CVD-grown MLG nanocomposite material. Cells were seeded at a concentration of 5 × 105 cells/mL on the prepared samples, which were incubated in a 5% CO_2 atmosphere at 37°C for 25 days. The prepared samples, cut into 1-cm discs, were sterilized by UV light for 30 min and then stored in commercial polystyrene tissue culture wells with DMEM/F12 culture medium supplemented with 10% FBS and 1% penicillin/streptomycin. Cell viability was determined by MTT assay, calcium deposition was assessed by Alizarin Red staining, and alkaline phosphatase activity was used to indicate differentiation. Adhesion and growth of seeded cells on the fabricated samples were analyzed using fluorescence microscopy and SEM. For general evaluation of cell culture, commercial polystyrene tissue culture mats and electrospun PVA mats were used as negative and positive controls.

MTT assay

The MTT (3-(4,5-dimethylthiazol-2-yl)-2,5-diphenyltetrazolium bromide) assay was used to assess cell viability on or in the prepared samples. The samples were incubated for 21 days in 24-well plates with prepared cell culture medium. After 24 hours, 7 days, 14 days, and 21 days, the inoculated samples were removed from the incubator, the medium was removed, and the samples were thoroughly washed three times with phosphate-buffered saline (PBS). Then, 60 μL of the MTT solution was mixed with 600 μL of fresh medium and added to each well. After a 3-h incubation period, the MTT solution was aspirated, and the formed formazan crystals were dissolved in 1 mL of dimethyl sulfoxide (DMSO) and incubated for an additional 1 h. A 200 μL aliquot was taken from each well and transferred to 96-well plates for cell viability measurement. Finally, absorbance values were measured using a microplate reader at 540 nm and cell viability was assessed.

ALP activity

The alkaline phosphatase (ALP) activity of the cultured samples was assessed after 7, 14, and 21 days. The substrate solution was prepared by dissolving the BCIP/NBT tablet in 10 mL of distilled water and storing it in the dark for 2 h. Then, the cultured samples were

taken out of the incubator, the cell medium was carefully aspirated, and the samples were washed three times with phosphate-buffered saline. The samples were then exposed to 10% formalin for 60 s to cover the surface. The formalin was then discarded, and the samples were thoroughly washed with PBS. The previously prepared substrate solution was added to the wells and incubated at room temperature for 10 min. Finally, the ALP activity was quantified by spectrophotometric measurement at 405 nm.

Alizarin Red staining

Alizarin Red S staining was performed to quantify calcium deposition by cultured cells on the prepared samples. A 2 g portion of Alizarin red stain was dissolved in 100 mL of distilled water, and the pH of the solution was adjusted to 4.1-4.3 with hydrochloric acid. The resulting deep brown solution was filtered and stored in the dark. After removing the samples from the incubator, the culture medium was carefully aspirated, and the cells were thoroughly washed with PBS without disturbing the cell monolayer. Then, the cells were fixed with 10% formalin solution. After 30 min of incubation, the formalin was carefully aspirated, and the cells were washed with distilled water. Then, Alizarin red staining solution was added to the samples and incubated in the dark for 30 min. Finally, the staining solution was centrifuged at 200 rpm, and the mineralization level was measured using a microplate reader.

Fluorescence microscopy

Fluorescence microscopy was conducted to examine cell attachment and proliferation on or within the samples. Specifically, the cultured samples were retrieved from the incubator, the medium was carefully removed, and the samples were then washed three times with PBS. Subsequently, the samples were immersed in a 0.1% Triton X-100 solution for five minutes to enhance cell permeability. The cells on or within the fabricated samples were stained with a 10 mg/mL DAPI solution and incubated in the dark for 15 min after discarding the Triton X-100 solution and washing the samples with PBS. Using a fluorescence microscope, images of the cultivated cells were captured immediately, with photographs taken on the 7th, 14th, and 21st days of cultivation.

RESULTS AND DISCUSSION

SEM analysis

SEM analysis was performed to investigate the morphology of PVA fibers of the prepared samples and the formation of graphene monolayer. Fig. 1 shows the SEM image of the electrospun PVA mat. The obtained fibers were smooth, without beads and uniform with interconnected pores. Furthermore, the formation and attachment of graphene monolayer to the electrospun PVA mat were studied using SEM and optical microscopy, and the obtained images are shown in Fig. 2. As shown in Figures 2a and 2b, the grain boundaries of CVD-produced MLG are clearly visible, while no grain boundaries can be seen on the Cu foil (after the peeling process), as expected. This ensures the transfer or attachment of graphene monolayer to the electrospun PVA mats. Moreover, according to Figures 2c and 2e, the adhesion of CVD-produced MLG to the electrospun PVA mats can be observed due to the peeling process, which is caused by the presence of partial CVD-produced MLG on the surface of the electrospun PVA mats. The average fiber diameters and pore sizes of the fabricated samples were determined using the Image J Launcher software and SEM. The exact process and solution parameters were used for the electrospinning of PVA for both fabricated nanocomposites. Thus, the average fiber diameter, pore size, and porosity values were statically similar ($p<0.0005$) for both samples, as in Table 1.

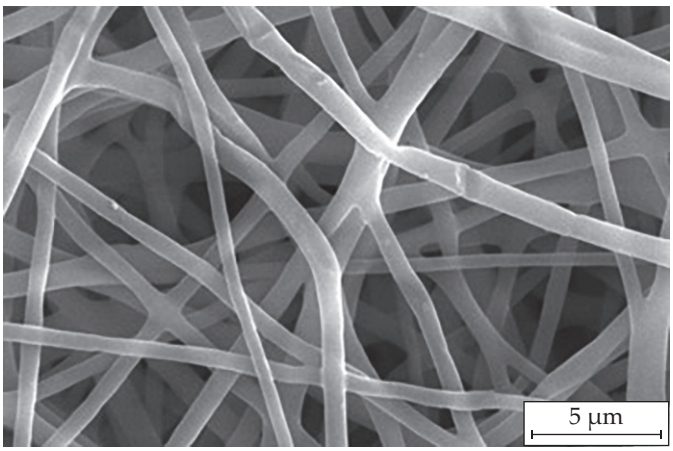

Fig. 1. SEM image of the electrospun PVA mat at 10000x magnification

Fig. 3 presents optical microscopy images of the CVD-grown MLG on Cu film before and after the peeling process. Figures 3a and 3b display the grain boundaries of the monolayer graphene on the Cu film. After the graphene transfer, no grain boundaries were visible on the Cu film, as shown in Figs. 3c and 3d. This observation has also been reported in other study [23]. Further characterization was performed using SEM to evaluate the quality of the graphene transfer, with the results detailed in the previous section.

T a b l e 1. Fiber diameter, pore size and porosity of the fabricated samples

Sample	Average fiber diameter, nm	Average pore size, μm	Porosity, %
PVA mat	335±6.0	1.068±0.120	79.4
PVA/CVD--grown MLG nanocomposite	332±1.0	1.052±0.020	79.1

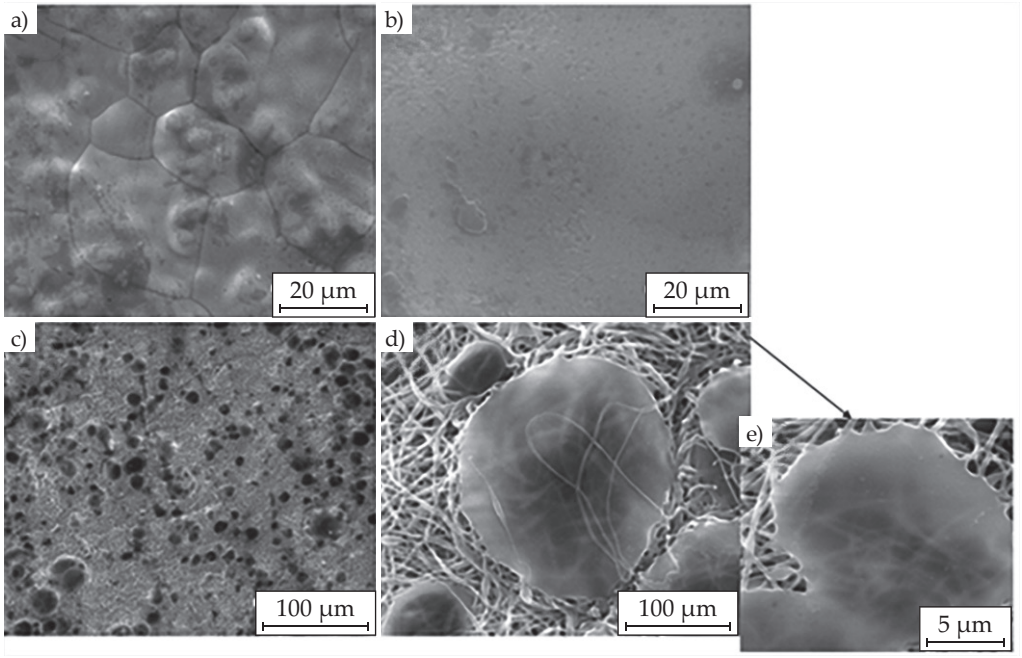

Fig. 2. SEM images: a) CVD-grown MLG on the Cu film, b) Cu film after peeling off, c, d, and e) PVA/CVD-grown MLG nanocomposite at different magnifications

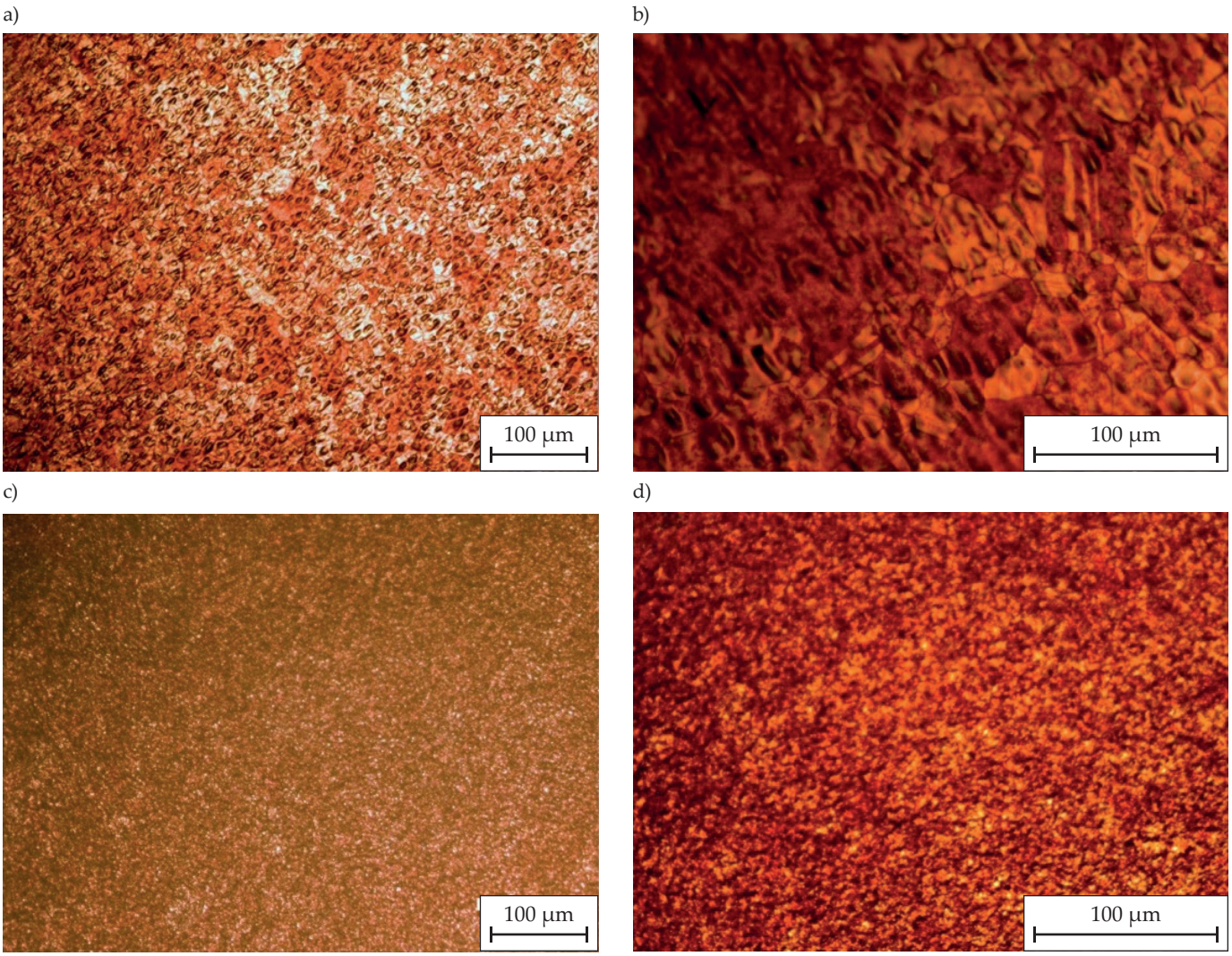

Fig. 3. Optical microscopy images of CVD-grown MLG at Cu film at various magnification: a) 40×, b) 100×, c) 40× after the peeling-off, d) 100× after the peeling-off

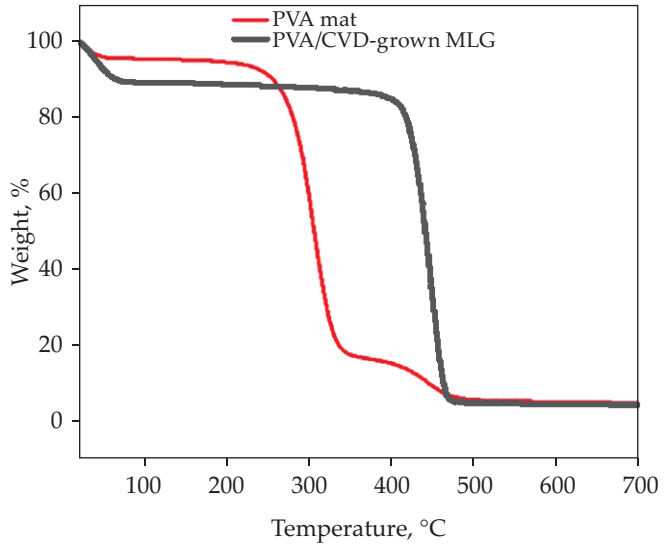

Fig. 4. TGA curves of PVA mat and PVA/ CVD-grown MLG

Tensile properties

The tensile properties of the electrospun PVA mat and PVA/CVD-grown MLG nanocomposite are presented in Table 2. PVA mat had tensile modulus of 1.210±0.004 MPa and tensile strength of 3.920±0.03 MPa, which aligns with typical electrospun PVA mat characteristics [24]. Similarly, the tensile properties of PVA/CVD-grown MLG nanocomposite were the same as those of the PVA mat. This could be due to the graphene monolayer's uneven distribution and weak attachment to the electrospun PVA mat.

T a b l e 2. Tensile properties of the fabricated nanocomposites

Sample	Tensile modulus, MPa	Tensile strength, MPa	Elongation at break, %
PVA mat	1.210±0.003	3.92±0.03	88.2±1.0
PVA/CVD-grown MLG nanocomposite	1.210±0.013	3.90±0.02	88.1±1.0

TGA analysis

Fig. 4 shows TGA curves of the electrospun PVA mat and PVA/CVD-grown MLG nanocomposite. The onset decomposition temperature and the maximum decomposition rate temperature of the nanocomposite were higher by 125°C and 140°C, respectively, indicating the higher thermal stability. TGA suggests that the deposition of graphene monolayer on the electrospun PVA mat enhanced the decomposition behavior of the electrospun structure [25]. This improvement is attributed to the physical barrier effect of graphene, which reduces the diffusion rate, as observed in other studies [26].

Raman spectroscopy analysis

Fig. 5 illustrates the Raman spectra of PVA mat, neat CVD-grown MLG, and PVA/CVD-grown MLG nanocomposite. The most prominent peak for electrospun PVA was observed at 2916 cm^{-1}, corresponding to CH_2 stretching in the PVA chain [27]. Additionally, peaks at 1172 cm^{-1} and 1444 cm^{-1} were credited to O-H and C-H vibrations, respectively [27]. The G band at 1581 cm^{-1} indicated the graphitic crystalline structure in the neat CVD-grown MLG spectrum, while the 2D band was visible at 2690 cm^{-1} [28]. For PVA/CVD-grown MLG nanocomposite, the CH_2 stretching at 2916 cm^{-1} and the O-H (1172 cm^{-1}) and C-H (1444 cm^{-1}) vibrations of PVA were also detected, though with lower intensity. The characteristic graphene bands at 1581 cm^{-1} (G) and 2690 cm^{-1} (2D) were similarly present. The IG/I2D ratio was calculated as 0.65 for neat graphene and 0.55 for the PVA nanocomposites with graphene, consistent with the literature [28]. This confirms the successful integration of the graphene layer into the electrospun PVA structure based on the Raman analysis.

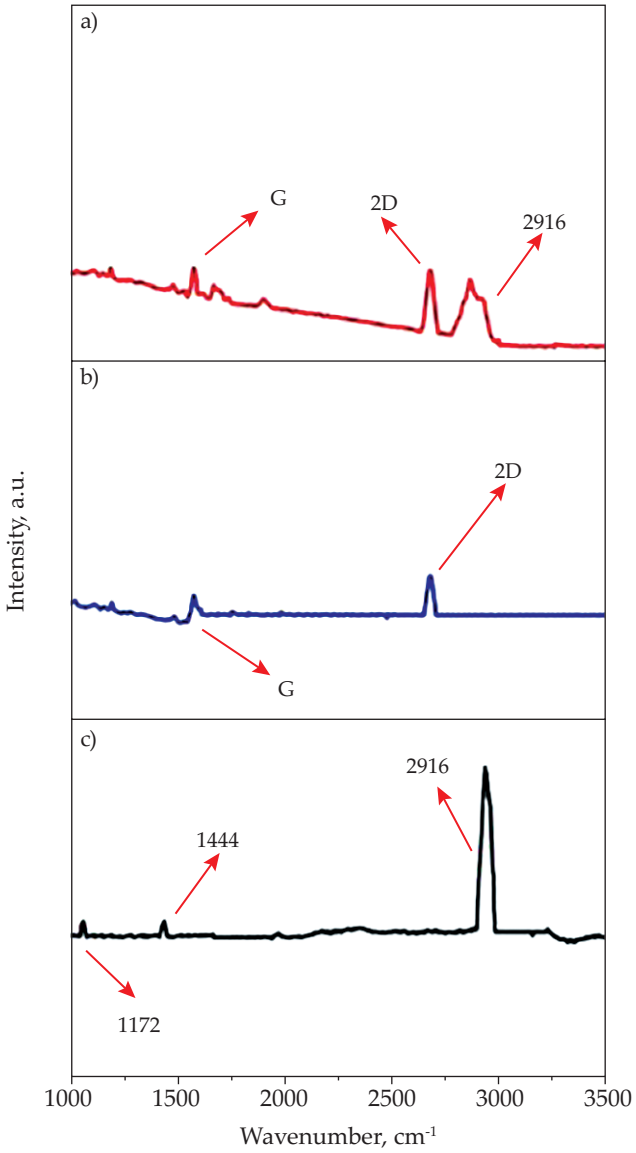

Fig. 5. Raman spectra: a) electrospun PVA mat, b) neat CVD-grown MLG, c) PVA/CVD-grown MLG nanocomposite

Electrical conductivity measurements

The electrical conductivity of the electrospun PVA mat and electrospun PVA/CVD-grown MLG nanocomposite was assessed using a 4-point probe device (Table 3). The conductivity of PVA/CVD-grown MLG nanocomposite increased in comparison with the pure electrospun PVA mat. This increase is due to the partial presence of monolayer graphene on the PVA mat, with the PVA matrix still dominating the overall structure.

T a b l e 3. Electrical conductivity and contact angle of PVA mat and PVA/CVD-grown MLG nanocomposite

Sample	Electrical conductivity, μS/cm	Contact angle, °
PVA mat	0.10±0.01	62.10±1.250
PVA/CVD-grown MLG nanocomposite	0.40±0.21	60.04±1.004

Contact angle measurements

Contact angle (CA) was measured to evaluate wettability, as shown in Table 3. Prior to crosslinking, electrospun PVA exhibited super-hydrophilic properties, making it impossible to obtain a CA measurement. However, after UV crosslinking, the CA of electrospun PVA was recorded at approximately 62°, which is attributed to the reorientation of hydroxyl groups [29]. In comparison, CA of PVA/CVD-grown MLG nanocomposite was found to be around 60°, reflecting the moderate wettability properties of CVD-grown MLG [22].

PBS absorption and shrinkage tests

The PBS absorption and shrinkage characteristics of the fabricated samples are shown in Table 4. Electrospun PVA mat exhibited lower PBS absorption (%) than PVA/CVD-grown MLG nanocomposite, due to their more hydrophobic nature. A similar pattern was observed in the shrinkage (%), as greater PBS absorption caused more shrinkage, altering the sample area.

T a b l e 4. PBS absorption and shrinkage

Sample	PBS absorption, %	Shrinkage, %
PVA mat	79.08±2.40	4.1±0.9
PVA/CVD-grown MLG nanocomposite	82.06±1.41	4.4±0.6

In vitro degradation

Fig. 6 illustrates the in vitro degradation of the electrospun PVA mat and PVA/CVD-grown MLG nanocomposite, depicting weight loss over time (30, 60, 90, and 120 days). The samples showed similar degradation patterns, which refer to the primary matrix for PVA mat and PVA/CVD-grown MLG.

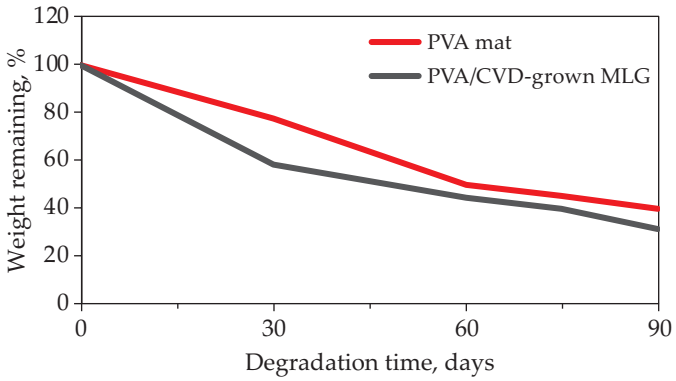

Fig. 6. Change in the mass of the tested samples over time

Water vapor transmission rate

Water vapor transmission rate (WVTR) is a measurement in which materials are compared for their ability to resist moisture transmission. WVTR of the electrospun PVA and PVA/CVD-grown MLG nanocomposite are shown in Fig. 7. Better permeability was observed for electrospun PVA mat, as WVTR decreased from 40 to 37 g/m^2·h for PVA/CVD-grown MLG nanocomposite. As the fiber diameter and fiber pore sizes were similar for both samples, the reason may be the partial location of monolayer graphene on the surface of electrospun PVA, which is exposed to water vapor. The monolayer graphene might close some of the open pores, which allows the vapor to be transmitted to the structure of electrospun PVA.

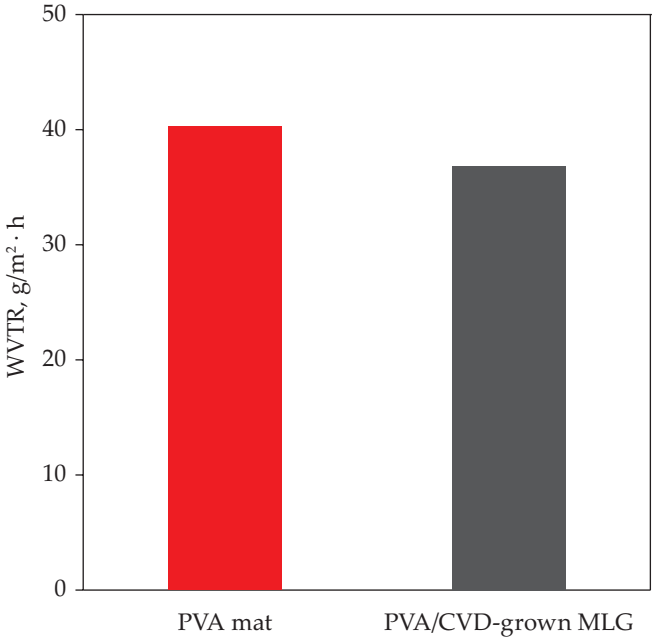

Fig. 7. WVTR of PVA mat and PVA/CVD-grown MLG nanocomposite

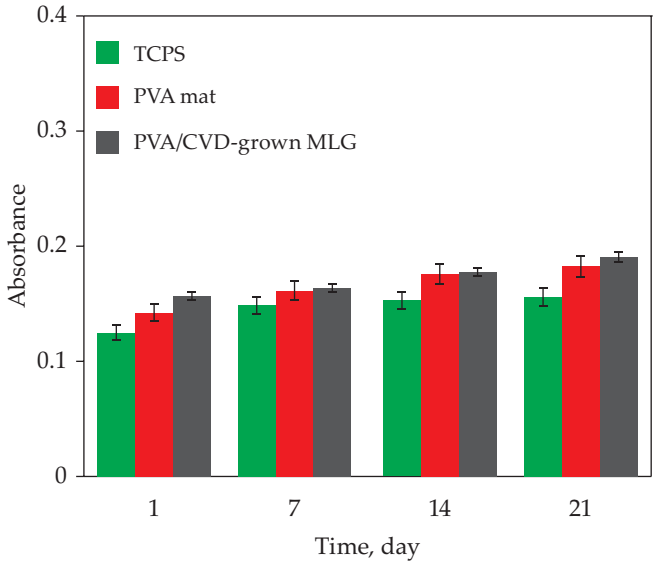

Fig. 8. Absorbance of PVA mat, PVA/CVD-grown MLG nanocomposite and TCPS by MTT

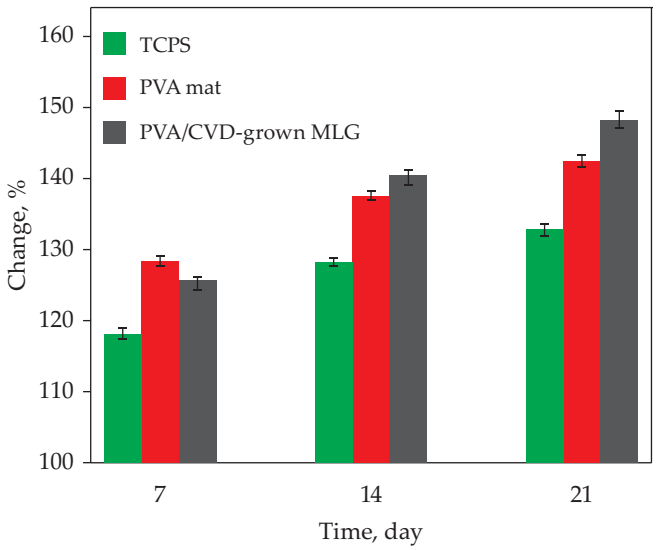

Fig. 9. ALP activity of the MG-63 osteosarcoma cells on the fabricated samples and TCPS (BCIP tablet was used as a blank substrate

Cell cultivation

MTT assay

Fig. 8 shows the results of the MTT assay, where the increase in absorbance over time indicates that electrospun PVA mat and PVA/CVD-grown MLG nanocomposite efficiently converted MTT into formazan during the 21-day incubation period [30]. Electrospun PVA mat displayed higher cell viability than the control TCPS, attributed to its 3D electrospun structure [31]. Meanwhile, the PVA/CVD-grown MLG nanocomposite exhibited slightly higher cell viability than both TCPS and the electrospun PVA mat, due to enhanced electrical conductivity [32].

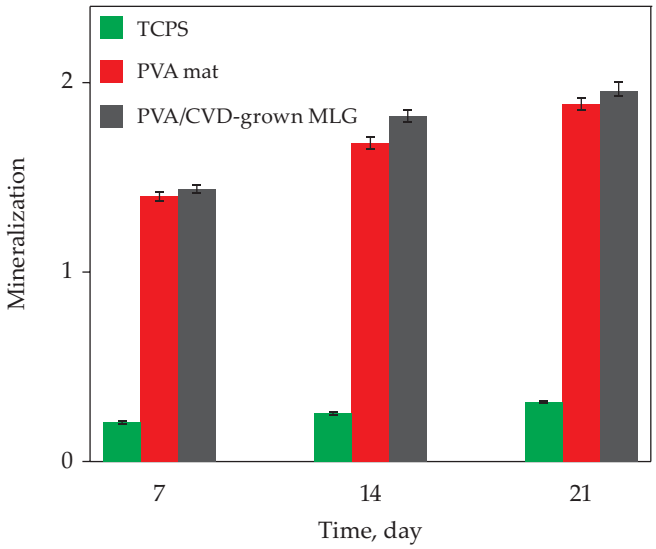

Fig. 10. Quantification of mineralization of MG-63 osteosarcoma cells cultured on samples prepared and TCPS

ALP activity

Alkaline phosphatase activity, which signifies early osteoblastic differentiation and inorganic phosphate accumulation [33], was assessed in MG-63 cells cultivated on electrospun PVA mat and PVA/ CVD-grown MLG nanocomposite. The percentage change in ALP activity after 7, 14, and 21 days of culture is presented in Fig. 9. Both samples supported better cell proliferation compared to TCPS, due to their 3D porous networks. However, the PVA nanocomposite with graphene monolayer supported even greater cell proliferation than the positive electrospun PVA mat and negative TCPS, consistent with the MTT assay results.

Alizarin-Red staining

Extracellular calcium deposition was evaluated on the TCPS, PVA mat, and PVA/CVD-grown MLG nanocomposite utilizing Alizarin Red staining. The assessment was conducted on the 7th, 14th, and 21st days of cell cultivation. Mineralization levels are displayed in Figure 10, with corresponding color changes shown in Fig. 11. Electrospun samples exhibited higher levels of mineralization than the TCPS control, due to their 3D structure. The highest mineralization level was shown in the PVA/CVD-grown MLG nanocomposite, as indicated by the most profound red staining, which is in line with the findings from the MTT assay and ALP activity studies.

Fluorescence microscopy analysis

Fluorescence microscopy was used to evaluate cell viability, adhesion, and proliferation on the fabricated samples after 7, 14, and 21 days of cell culture (Fig. 12). Cell viability and adhesion increased over time in all the samples

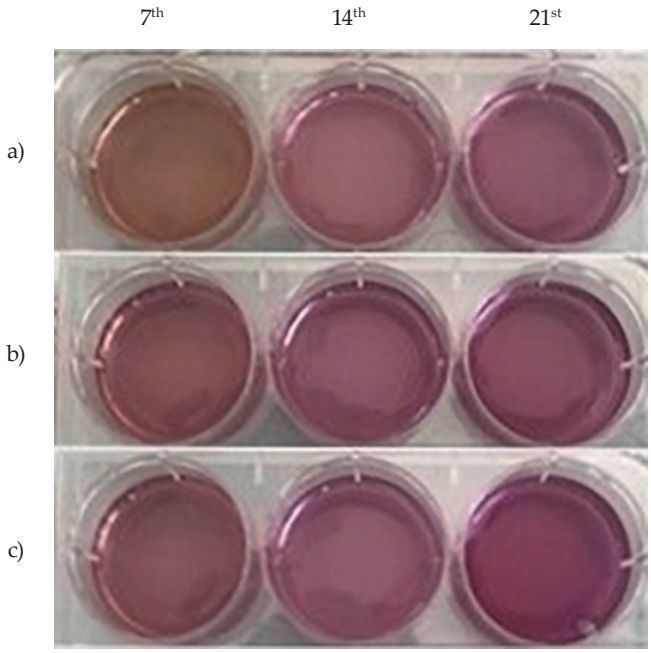

Fig. 11. The color change is due to Ca^{+2} deposition: a) TCPS, b) PVA mat, c) PVA/CVD-grown MLG

tested. As observed by MTT assay, ALP activity, and Alizarin Red staining, the PVA/CVD-grown MLG nanocomposite showed the highest cell population throughout the culture period.

CONCLUSIONS

CVD-grown MLG was successfully transferred from Cu film to electrospun PVA using a non-etching technique. The developed nanocomposite showed enhanced electrical conductivity, significantly improved thermal stability, and slightly enhanced wettability, which resulted in improved PBS absorption. Moreover, partial attachment of monolayer graphene on the surface of electrospun PVA mat, which was exposed to water vapor, could close some of the open interconnected pores, which enabled vapor transmission. Consequently, a lower WVTR value was observed for the PVA/CVD-grown MLD nanocomposite. *In vitro* degradation studies showed that the PVA mat and the PVA/CVD-grown MLD composite had similar degradation behavior in PBS. Moreover, cell culture studies including MTT analysis, ALP activity, Alizarin Red staining, and fluorescence microscopy analysis proved that the PVA/CVD-grown MLG nanocomposite was more biocompatible than the PVA mat, and it was concluded that the developed PVA/CVD-grown MLG nanocomposite was suitable for scaffold-based tissue engineering.

ACKNOWLEDGMENT

Veera Bhadraiah Sadhu acknowledges FCT - Fundação para a Ciência e a Tecnologia and University of Beira Interior for the research contract CEECINST/00016/2021/CP2828/CT0007 under the scope of the CEEC Institutional 2021, funded by FCT.

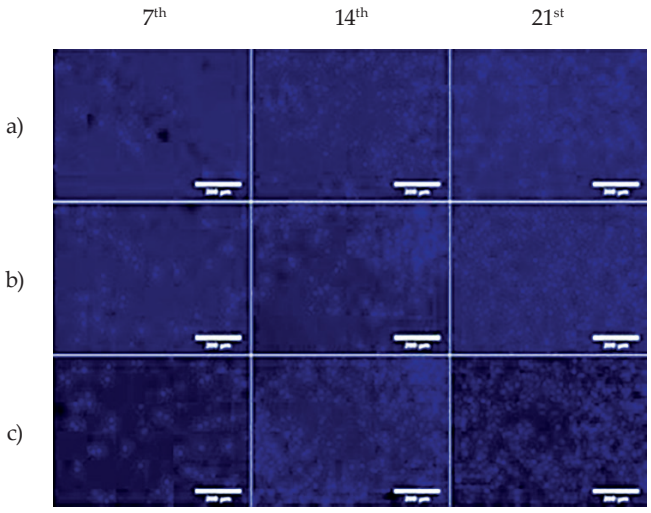

Fig. 12. Fluorescence images (by DAPI stain): a) TCPS, b) PVA mat, c) PVA/CVD-grown MLG

Authors contribution

H.T.S. – conceptualization, methodology, validation, supervision, writing-review, and editing; M.A. – methodology, formal analysis, writing-review, and editing; V.S. – conceptualization, methodology, validation; M.G. – methodology, formal analysis, validation, investigation, writing-original draft.

Funding

Veera Bhadraiah Sadhu acknowledges FCT - Fundação para a Ciência e a Tecnologia and University of Beira Interior for the research contract CEECINST/00016/2021/CP2828/CT0007 under the scope of the CEEC Institutional 2021, funded by FCT.

Conflict of interest

The authors declare no conflict of interest.

REFERENCES

[1] Albayrak D., Sasmazel H.T.: *Journal of Polymer Research* **2022**, *29*, 339. https://doi.org/10.1007/s10965-022-03164-6

[2] Alazzawi M., Alsahib N.K.A., Sasmazel H.T.: *Coatings* **2021**, *11(9)*, 1130. https://doi.org/10.3390/coatings11091130
[3] Puigmal A.C., Ayran M., Ulag S. *et al*.: *Journal of the Mechanical Behavior of Biomedical Materials* **2023**, *148*, 106163. https://doi.org/10.1016/j.jmbbm.2023.106163
[4] Sharma N., Dev Gupta R., Sharma R.C. *et al*.: *Materials Today. Proceedings* **2021**, *47(11)*, 2752. https://doi.org/10.1016/j.matpr.2021.03.086
[5] Worku A.K., Worku Ayele D.: *Results in Chemistry* **2023**, *5*, 100971. https://doi.org/10.1016/j.rechem.2023.100971
[6] Ahmad F., Zihad M., Jamil H. *et al*.: *Journal of Energy Storage* **2023**, *72(E)*, 108731. https://doi.org/10.1016/j.est.2023.108731
[7] Dong X., Shi Y., Huang W. *et al*.: *Advanced Materials* **2010**, *22(14)*, 1649. https://doi.org/10.1002/adma.200903645
[8] Jaaniso R., Kahro T., Kozlova J. *et al*.: *Sensors and Actuators B: Chemical* **2014**, *190*, 1006. https://doi.org/10.1016/j.snb.2013.09.068
[9] Alazzawi M., Sasmazel H.T.: "Materials and Processes for Treatment of Microbiological Pollution in Water" in "Water Safety, Securiy and Sustainability", (Editors: Vaseashta A., Maftei C.), Springer Nature Switzerland, Cham 2021. p. 291. https://doi.org/10.1007/978-3-030-76008-3_13
[10] Syama S., Mohanan P.V.: *Nano-Micro Letters* **2019**, *11*, 6. https://doi.org/10.1007/S40820-019-0237-5
[11] Al Faruque M.A., Syduzzaman M., Sarkar J. *et al*.: *Nanomaterials* **2021**, *11(9)*, 2414. https://doi.org/10.3390/nano11092414
[12] Hakami M.A.: "Graphene Growth by Chemical Vapor Deposition," MS Thesis, King Abdullah University of Science and Technology, Thuwai 2019. https://doi.org/10.25781/KAUST-91OSQ
[13] Ali S., Ahmad F., Yusoff P.S.M.M. *et al*.: *Composites Part A: Applied Science and Manufacturing* **2021**, *144*, 106537. https://doi.org/10.1016/j.compositesa.2021.106357
[14] Osikoya A.O., Parlak O., Murugan N.A. *et al*.: *Biosensors and Bioelectronics* **2017**, *89(1)*, 496. https://doi.org/10.1016/j.bios.2016.03.063
[15] Ji Q., Shi L., Zhang Q. *et al*.: *Applied Surface Science* **2016**, *387*, 51. https://doi.org/10.1016/j.apsusc.2016.06.086
[16] Vatanpour V., Teber O.O., Mehrabi M. *et al*.: *Materials Today. Chemistry* **2023**, *28*, 101381. https://doi.org/10.1016/j.mtchem.2023.101381
[17] Barzegar F., Bella A., Faibiane M. *et al*.: *Journal of Physics and Chemistry of Solids* **2015**, *77*, 139. https://doi.org/10.1016/j.jpcs.2014.09.015
[18] Xie H., Chua M., Islam I. *et al*.: *Dental Materials* **2017**, *33(1)*, e13. https://doi.org/10.1016/j.dental.2016.09.030
[19] Rezaei M., Li S., Huang S. *et al*.: *Journal of Membrane Science* **2020**, *612*, 118406. https://doi.org/10.1016/j.memsci.2020.118406
[20] Rahman L., Goswami J.: *Journal of Packaging Technology and Research* **2023**, *7*, 1. https://doi.org/10.1007/s41783-022-00146-3
[21] ASTM International: "ASTM E96: Standard Test Methods for Water Vapor Transmission of Materials," in "Annual Book of ASTM Standards", West Conshohocken 1995. p. 785.
[22] Rezaee O., Chenari H.M., Ghodsi F.E. *et al*.: *Journal of Alloys and Compounds* **2017**, *690*, 864. https://doi.org/10.1016/j.jallcom.2016.08.212
[23] Marta B., Leordean C., Istvan T. *et al*.: *Applied Surface Science* **2016**, *363*, 613. https://doi.org/10.1016/j.apsusc.2015.11.265
[24] Bazzi M., Shabani I., Mohandesi J.A.: *Journal of the Mechanical Behavior of Biomedical Materials* **2022**, *125*, 104975. https://doi.org/10.1016/j.jmbbm.2021.104975
[25] Shui Y.J., Yao W.H., Lin J.H. *et al*.: *Polymers* **2024**, *16(8)*, 1070. https://doi.org/10.3390/polym16081070
[26] Berry V.: *Carbon* **2013**, *62*, 1. https://doi.org/10.1016/j.carbon.2013.05.052
[27] Mohd Abdah M.A.A., Zubair N.A., Azman N.H.N. *et al*.: *Materials Chemistry and Physics* **2017**, *192*, 161. https://doi.org/10.1016/j.matchemphys.2017.01.058
[28] Jiang Y., Sun Y., Song J.: *Micron* **2017**, *97*, 29. https://doi.org/10.1016/j.micron.2017.03.005
[29] Gozutok M., Sadhu V., Sasmazel H.T.: *Journal of Nanoscience and Nanotechnology* **2019**, *19(7)*, 4292. https://doi.org/10.1166/jnn.2019.16290
[30] Topsakal A., Uzun M., Ugar G. *et al*.: *IEEE Transactions on NanoBioscience* **2018**, *17(3)*, 321. https://doi.org/10.1109/TNB.2018.2844870
[31] Gozutok M., Baitukha A., Arefi-Khonsari F. *et al*.: *Journal of Physics D: Applied Physics* **2016**, *49*, 474002. https://doi.org/10.1088/0022-3727/49/47/474002
[32] Topsakal A., Midha S., Yuca E. *et al*.: *Materials Today. Communications* **2021**, *28*, 102458. https://doi.org/10.1016/j.mtcomm.2021.102458
[33] Sasmazel H.T.: *International Journal of Biological Macromolecules* **2011**, *49(4)*, 838. https://doi.org/10.1016/j.ijbiomac.2011.07.022

Received 17 X 2024.
Accepted 31 X 2024.